Journal of Molecular Catalysis A: Chemical 324 (2010) 9–14

Contents lists available at ScienceDirect

Journal of Molecular Catalysis A: Chemical

journal homepage: www.elsevier.com/locate/molcata

Computational catalysis

On the mechanism of the rhodium catalyzed acrylamide hydrogenation☆

Vincenzo Verdolino[a], Aaron Forbes[a], Paul Helquist[a], Per-Ola Norrby[b], Olaf Wiest[a,*]

[a] Department of Chemistry and Biochemistry, University of Notre Dame, Notre Dame, IN, 46556-5670, United States
[b] Department of Chemistry, University of Gothenburg, SE-412 96 Göteborg, Sweden

ARTICLE INFO

Article history:
Available online 1 March 2010

Keywords:
Hydrogenation
Mechanism
Electronic structure
Rhodium

ABSTRACT

The hydrogenation of acrylamides using chiral Rh(I) complexes is an attractive method for the enantioselective synthesis of highly functionalized intermediates. It has been employed less frequently than the related Rh(I) catalyzed hydrogenation of enamides and the mechanism of the reaction is not well understood. The parent reaction of acrylamide with a simple Rh(I) bisphosphine complex was studied at the B3LYP/LanL2TZ(f)/6–31++G** level of theory and shows a number of interesting differences compared to the mechanism of the enamide reaction. The minimum energy reaction pathway was found to involve attack of the molecular hydrogen parallel to the C–Rh–P bond, followed by an isomerization at the stage of the dihydride complex to give an altered orientation of the hydride, which is then transferred to the β-carbon.

1. Introduction

Acrylamide reduction *via* catalytic hydrogenation, shown in Fig. 1, is a very attractive reaction having several important applications in the synthesis of chiral α- and/or β-substituted amides, esters, and carboxylic acids. As of yet this reaction is not as widely used, nor the mechanism as well understood as the corresponding hydrogenation of the analogous enamide system [1], which has been mechanistically studied in great detail [2–8]. As a result, there is no clear basis for the selection of chiral ligands and catalysts for optimum enantioselectivity in asymmetric versions of the reaction.

Keinan and co-workers [9] have developed a reducing system comprised of phenylsilane and catalytic amounts of $Mo(CO)_6$ that efficiently reduces the C–C bond of α,β-unsatured carbonyl compounds. A variety of acrylamide substrates are selectively reduced to the saturated amides in yields between 70% and 100%. Koltunov and co-workers [10] explored the electrophilic reactivity of α,β-unsatured amides with weak nucleophiles catalyzed by superacids. The authors showed that some substrates undergo selective transfer hydrogenation to give saturated amides suggesting dicationic electrophiles as an explanation of the reaction mechanism. Brubaker and co-workers [11] presented a highly chemo- and regioselective catalytic reduction of a carbon-carbon double bond conjugated to different unsaturated functional groups, including amides. Ferrocenylamine sulfide complexes of Pd(II) were particularly effective, giving in many cases yields and chemoselectivities of >99%. However, the stereoselectivity of the reduction of prochiral substrates was not investigated. The most promising method for the enantioselective hydrogenation of the carbon-carbon bond of α,β-unsatured carbonyls is the use of Rh(I) catalysis, which has been successfully applied to acrylic acids and esters. Early work by Hayashi resulted in e.e.'s of up to 98% [12]. More recently, Sturm, et al. [13,14] used a series of Rh(I) Walphos complexes in the asymmetric hydrogenation of α,β-unsatured esters, obtaining up to 95% e.e. However, applications of these catalytic systems to the enantioselective reduction of α,β-unsaturated amides have been rare [15], even though there are examples of their hydrogenation under non-enantioselective conditions [16].

This prior work demonstrates the utility of the hydrogenation of acrylamides, but there has been very little work concerning the mechanism of the hydrogenation of α,β-unsaturated carboxylic acid derivatives in general [17]. This lack of mechanistic insight is unfortunate because a detailed understanding of the mechanism of a reaction is a prerequisite for the rational development of synthetically useful enantioselective versions of a reaction. Indeed, our previous work on the Rh(I) catalyzed hydrogenation of enamides demonstrates that the enantioselectivity of the reduction can be quantitatively predicted based on an understanding of the stereoselecting transition structures using the Q2MM method [5–7]. In these previously studied reactions, four possible pathways based on the approach of molecular hydrogen to the substrate-catalyst complex were considered. We therefore decided to investigate the four corresponding pathways for the Rh(I) catalyzed hydrogenation of acrylamides for a simple achiral model system to identify the transition structures, the rate determining step of the reaction, and to compare this reaction to the better understood enamide hydrogenation. The knowledge gained from this study is a neces-

☆ This paper is part of a special issue on Computational Catalysis.
* Corresponding author.
E-mail addresses: owiest@nd.edu, Olaf.G.Wiest.1@nd.edu (O. Wiest).

1381-1169/$ – see front matter © 2010 Elsevier B.V. All rights reserved.
doi:10.1016/j.molcata.2010.02.026

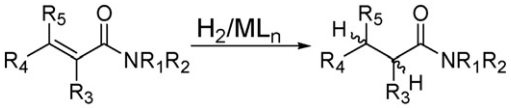

Fig. 1. Acrylamide hydrogenation.

sary building block for later studies of enantioselective versions of this reaction.

2. Computational methodology

We performed a computational study at the B3LYP [18] level of theory in the gas phase to characterize the intermediates and transition states involved in the reaction. All calculations were performed using a 6–31++G** basis set on non-metal atoms and the LanL2TZ(f) basis set with an ECP [19–21] effective core potential on the Rh atom. Unlike in previous studies by Landis and co-workers [22], we found the larger LanL2TZ(f) basis set necessary for the optimization of the **SQPL** and **MOLH2** structures (for nomenclature of the species, see Fig. 2). This is presumably because of the more constrained four- to five-membered ring system formed by the chelation of the acrylamide to the metal, which requires a more flexible basis set compared with five- to six-membered ring in the enamide system. No symmetry or coordinate constraints were applied except where noted, and all stationary points were characterized as minima or transition structures by harmonic frequency analysis. All calculations were performed with Gaussian03 [23]. Reported energies are Gibbs free energies under standard conditions in kcal/mol and are relative to the energy of the separated complexes and hydrogen.

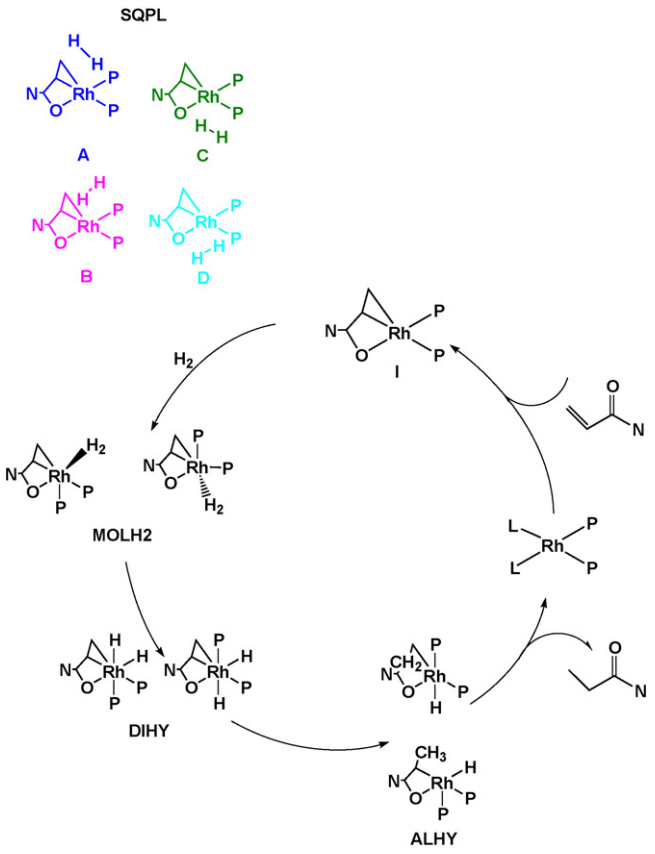

Fig. 2. Proposed mechanism for the Rh(I) catalyzed acrylamide hydrogenation.

Table 1
Structural parameters of the acrylamide–rhodium **SQPL** complex and comparison with analogous computational and experimental data for the enamide–rhodium complex.

Parameter	SQPL-A	SQPL-A/B[a]	Exptl.-1[b]
Bonds (Å)			
Rh–O	2.16	2.11	2.11
Rh–Ca	2.19	2.17	2.20
Rh–Cb	2.18	2.15	2.25
Rh–P_{trans}O	2.26	2.38	2.23
Rh–P_{trans}C	2.37	2.47	2.27
C_α–C_β	1.40	1.44	1.38
Angles (°)			
O–Rh–Ca	64.3	79.0	77.8
Ca–Rh–P_{cis}	106.4	99.7	109.6
P–Rh–P	94.1	94.1	83.0
O–Rh–P_{cis}	94.9	87.5	88.9
Ca–Rh–Cb	37.5	38.3	36.2

[a] Computational data for $[Rh(PH_3)_2(\alpha\text{-acetamidoacrylonitrile})]^+$ from Ref. [22].
[b] X-ray structure of [Rh(DIPHOS)(methyl-(*Z*)-R-acetamidocinnamate)](BF_4) data from Refs. [24,25].

3. Results and discussion

We consider in this study a model system consisting of an achiral catalyst and a simple acrylamide substrate ($R_1 = R_2 = R_3 = R_4 = R_5 = H$) shown in Fig. 1. The starting point of the process is the complex **SQPL**, the adduct consisting of a rhodium(I) with two cis-ligated $-PH_3$ ligands and a coordinated acrylamide moiety. This minimal system represents the essential features of the previously studied systems [12–14,16] as well as the systems we plan to study experimentally in our future investigations.

In analogy to the computational studies of the enamide hydrogenation, we considered four possible pathways, termed A–D in the remainder of the paper and defined in Fig. 2, where molecular hydrogen approaches the catalyst parallel to the P–Rh–C or to the P–Rh–O bond either from above or below the square plane. Each of the four pathways involves the following species as well as the transition structures connecting them: (1) the square planar precursor **SQPL** and isolated molecular hydrogen, (2) induced dipole complex of H_2 interacting with **SQPL**, (3) tri-center molecular hydrogen complex (**MOLH2**), (4) dihydride complex (**DIHY**), and (5) alkyl hydride complex (**ALHY**). All structures will be identified in the paper by these abbreviations, followed by the letter indicating the pathway they belong to.

3.1. Structure of *SQPL* complex

To the best of our knowledge, no crystal structure describing the acrylamide–rhodium complex analogous to the model under study has been reported in the literature. However, it is a reasonable hypothesis that the previously studied enamide–rhodium complexes share many of their essential features with the acrylamide complexes and serve to highlight significant similarities or differences between the two classes of complexes. Several structures of $[Rh(enamide)(diphosphine)]^+$ complexes have been published, and most of them involve bidentate phosphine ligands [24–26]. Table 1 compares our computational results for **SQPL** with the essential geometric parameters of the crystal structure of [Rh(DIPHOS)-(methyl-(Z)-α-acetamidocinnamate)](BF_4) [25], and the computational results of Landis et al. [22] for the square planar complex in their studies of enamide hydrogenation, obtained at a similar level of theory.

The structure of **SQPL-A** is representative of the other **SQPL** complexes and will be discussed here. The overall comparison of the most relevant bond lengths and angles shows the analogies between the acrylamide and enamide rhodium complexes

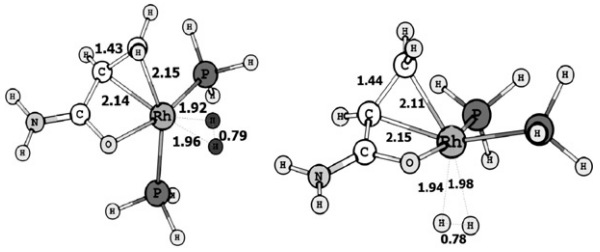

Fig. 3. Calculated structures of **MOLH2-A** (left) and **MOLH2-C** (right).

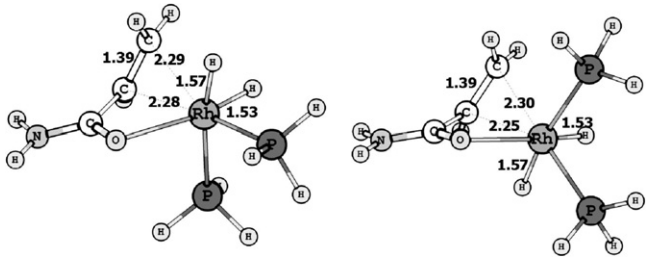

Fig. 4. Calculated structures of **DIHY-B** (left) and **DIHY-D** (right).

and demonstrates the coordination of the rhodium to the oxygen and the olefin in a bidentate fashion. The geometric parameters for the coordinating double bond moiety are consistent with previous computational and experimental data. The optimized C_α=C_β bond length is 1.40 Å, and the C_α–Rh–C_β angle is 37.5°, which are in good agreement with 1.38 Å and 36.2° for the enamide–rhodium crystal structure. The key difference between the structures is a stretched O–Rh bond distance, which is 2.16 Å in the acrylamide–rhodium complex, compared with 2.11 Å optimized for the enamide–rhodium analog. This result is easily explained considering the principal difference between these two coordinating systems: the acrylamide substrate is forced to coordinate in a four-membered ring, which results in more strain than the five-membered ring that characterizes the enamide substrate. As expected, the *trans* influence of the olefin coordination on the Rh–P_{trans} bond length is reproduced well, giving a bond length of 2.36 Å which is significantly longer than the 2.26 Å distance between rhodium and the phosphorus *trans* to the carbonyl function. It is noteworthy that the **SQPL** potential energy surfaces are very flat in all four cases, suggesting significant flexibility for H–H rotation with respect to the approaching plane.

3.2. The molecular hydrogen complex

The optimization of the four stable intermediates for the coordinated molecular hydrogen complexes gave the structures **MOLH2-A**, **MOLH2-C**, and **MOLH2-B/D**, the first two of which are shown in Fig. 3. The optimized structure of **MOLH2-A** shows a near ideal trigonal bipyramidal coordination with the amido oxygen in an axial position. The key Rh–hydrogen interaction in both structures has a bond length of >1.9 Å, which is significantly weaker than in the case of the enamides [3]. **MOLH2-A** has a calculated relative free energy of 12.8 kcal/mol, which is less stable than **MOLH2-C** by 1.7 kcal/mol. However, both of these structures are significantly more stable than the alternative approach of the dihydrogen parallel to the P–Rh–O bond in **MOLH2-B/D** that lead to a trigonal coordination of the molecular H_2 in the *trans* position with respect to the amido oxygen instead of the phosphine (see structure in Supporting Information). The *trans* effect results in a significant shortening of the Rh–H_2 distance in the **MOLH2-B/D** with respect to the other two structures, and consequently the two phosphines become equivalent in terms of the Rh–P distance. In analogy to the enamide reaction [22], this structure is accessible from both the **SQPL-B** and the **SQPL-D** approach of the hydrogen. In agreement with the least motion principle [27] and the results for the enamide case [3,7], the **MOLH2-B/D** intermediate is kinetically inaccessible and will therefore not be considered at this point as a likely intermediate.

3.3. Metal dihydrides

Unlike the **MOLH2** structures, which converge for the B and the D pathways, four distinct structures for the dihydrogen complex **DIHY** were located. Fig. 4 shows the two low-energy isomers, **DIHY-B** and **DIHY-D** with relative free energies of 11.9 and 11.3 kcal/mol, respectively. The structures for the two alternative complexes

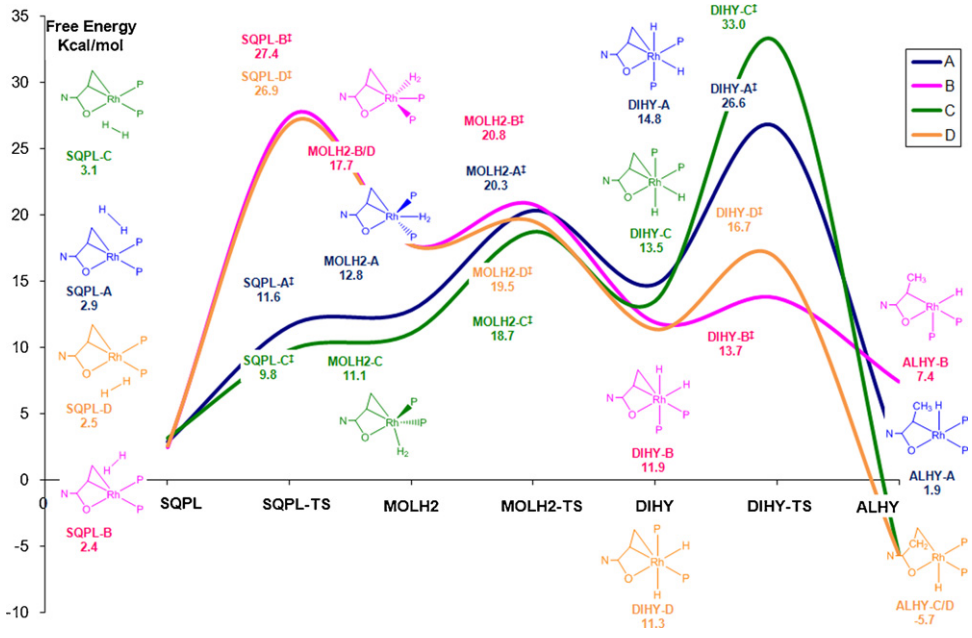

Fig. 5. Reaction PES profile for the A–D pathways.

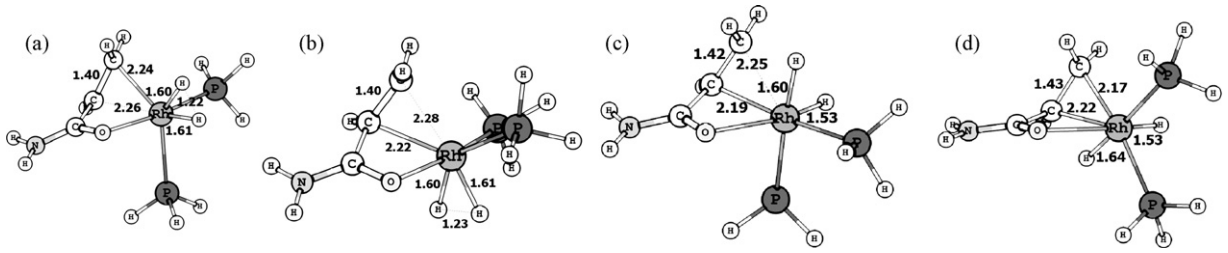

Fig. 6. Structures of (a) **MOLH2-A**‡, (b) **MOLH2-C**‡, (c) **DIHY-B**‡ and (d) **DIHY-D**‡ with selected geometric parameters.

DIHY-A and **DIHY-C**, which are 2–3 kcal/mol higher in energy, are given in the Supporting Information. In all cases, one hydrogen is positioned *trans* to a phosphine and the other *trans* to the amido oxygen (B and D pathways) or to the olefin (A and C). The *trans*-positions of the hydride and the phosphine in **DIHY-B** and **DIHY-D** lead to the slightly lower relative free energy of these two structures [22]. It is noteworthy that the two low-energy structures for **DIHY** belong to a different pathway than the ones for **MOLH2**, which has significant consequences for the overall reaction mechanism.

3.4. The reaction pathways for the hydrogenation of acrylamide

Unlike in the case of the enamides, the energy profile of the acrylamide reaction pathway does not necessarily exclude any of the four possible mechanisms. We therefore calculated the relevant transition structures along the pathways **A–D**. The results of these calculations are summarized in Fig. 5.

Qualitatively, the reaction pathways share many features with the mechanism of the enamide hydrogenation, but the relative energies of the intermediates and transition structures involved are substantially higher. This reflects the higher ring strain of the chelate as well as the lack of a second acceptor substituent in our model system, resulting in a lack of stabilization for the negative charge developing on the substrate in the later stages of the reaction. The two transition states **SQPL-A**‡ and **SQPL-C**‡ have a relative free energy of 11.6 and 9.8 kcal/mol, respectively. This part of the potential energy surface is so flat that after correction for zero-point energy, the transition state and respective products are essentially isoenergetic.

Two different transition states **SQPL-B**‡ and **SQPL-D**‡ lead to the common intermediate **MOLH2-B/D** and have a relative free energy of approximately 27 kcal/mol. The localization of these two structures turned out to be quite cumbersome, and in the case of **SQPL-B**‡, required the use of a dihedral constraint in order to avoid the isomerization into the A pathway. Similarly, many of the attempts to locate **SQPL-D**‡ led to an isomerization to the C pathway. In either case, the calculated transition structures are high enough in energy to make these pathways kinetically inaccessible and restrict an approach along the P–Rh–C axis.

The four possible transition structures for the oxidative addition to the dihydride complex, **MOLH2-A-D**‡, were found to be very close in energy. With a range of relative free energies of 18.7–20.8 kcal/mol, the differences between them is on the order of the accuracy that can reasonably be expected for the level of theory used here, and no determination of the preferred pathway can be made based on the relative energies of these transition structures. Fig. 6 shows on the left two representative transition state structures, (a) **MOLH2-A**‡ and (b) **MOLH2-C**‡. As expected, the overall geometry reflects the coordination change from the trigonal bipyramid for **MOLH2** to the octahedral coordination of **DIHY** with two nearly identical Rh–H bonds and, in comparison to the enamide analogs, longer C–Rh bonds for the reasons discussed above.

In the case of the enamide hydrogenation, we previously argued that the transition structures for the hydride transfer **DIHY**‡ determines the stereoselectivity of the reaction because a Q2MM transition state force field (TSFF) derived from these structures accurately describes the stereoselectivity of the reaction, whereas a TSFF derived from the **MOLH2** structures does not [5,6]. Furthermore, the stability of the developing negative charge determines whether the hydride is preferentially transferred to the α or β carbon [7]. Because the amide is the only acceptor in the model system studied here, hydride transfer to the β carbon with development of the negative charge on the α-carbon where it can be stabilized is preferred by 3 and 6.3 kcal/mol in both the B and the A pathways, respectively. In comparison, the transition structures for the A and the C pathways **DIHY-A**‡ and **DIHY-C**‡ are with relative free energies of 26.6 and 33.0 kcal/mol, respectively, kinetically inaccessible for the model system studied here. Fig. 6 shows on the right the two low-energy transition structures for the transfer of the hydride to the α or β carbon, (c) **DIHY-B**‡ and (d) **DIHY-D**‡. In agreement with the strongly exothermic character of this step, the carbon-hydrogen bonds are, with bond distances of 1.59 and 1.67 Å in **DIHY-B**‡ and **DIHY-D**‡, only weakly formed and the C–Rh distance does not change substantially from the corresponding **DIHY** intermediates.

The hydrogen transfer process irreversibly leads to the alkyl hydride products, which in this study will be considered as the final stage of the reaction. A variety of alkyl hydride compounds can be obtained from the migratory insertion process: three products arise directly from the respective dihydride intermediates: **ALHY-A** with a relative free energy of 1.9 kcal/mol, the **ALHY-B** with a relative free energy of 7.4 kcal/mol, and **ALHY-C/D**, a common product of the C and D pathways through a hydrogen transfer onto the α carbon with a relative free energy of −5.7 kcal/mol.

Taken together, these results provide an incomplete picture of the reaction pathway because the high energy of the **SQPL-B**‡ and **SQPL-D**‡ transition structures precludes the formation of the analogous molecular hydrogen complexes **MOLH2-B** and **MOLH2-D**, while the high free energies of **DIHY-A**‡ and **DIHY-C**‡ make this pathway also inaccessible under the experimentally used conditions. This seeming contradiction can be resolved under the assumption that a crossing over between the pathways is possible, either at the stage of **MOLH2** or **DIHY**. We therefore performed the transition state search for an isomerization pathway between **MOLH2-B** and **MOLH2-D**. If such a transition state exists, its energy must be lower than the two predicted **SQPL-B**‡ and **SQPL-D**‡ transition states in order to be mechanistically relevant, and the geometry relaxation from the two *minima* following the intrinsic reaction path (IRC) must converge in both cases to the **MOLH2-B/D** intermediate. In agreement with the previously mentioned finding that this intermediate easily optimized to other structures, we were able to locate the transition structure for the isomerization pathway with a unique imaginary frequency (357 cm^{-1}), which describes the H–H bond rotation with respect to the Rh–O bond direction. The relative free energy of this transition state is 20.2 kcal/mol, approximately 7 kcal/mol lower in energy than the relative **SQPL**‡ transition states and just 2 kcal/mol higher than **MOLH2-B/D**. The identity of this transition structure was confirmed by IRC calculation leading to

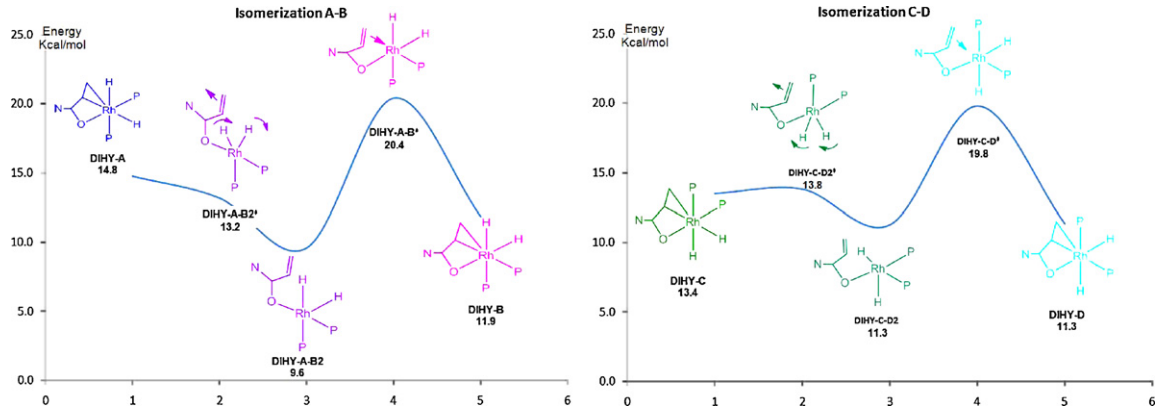

Fig. 7. Energy profile for dihydride isomerization of **DIHY-A** into **DIHY-B** (left) and **DIHY-C** into **DIHY-D** (right).

two minima that can be associated with **MOLH2-B** and **MOLH2-D**, respectively, but unconstrained relaxation of both geometries converges in a common structure that matches **MOLH2-B/D**. However, we were unable to locate a transition structure for the isomerization of the A and the B or the C and the D pathways at the stage of **MOLH2**.

We therefore studied the energy profile for the isomerization pathway of **DIHY-A** → **DIHY-B** and **DIHY-C** → **DIHY-D**, shown in Fig. 7. The isomerization process occurs in two steps: (1) the olefin dissociates while the H–Rh–H angle rotates around the O–P_{trans} direction, and (2) translation of the oxygen to the vacant site and coordination of the olefin double bond to the metal. The overall relative free energy barrier is 20.4 and 19.8 kcal/mol, respectively, for the A → B and C → D isomerization. The isomerization process represents an important side path of this reaction: contrary to the enamide hydrogenation reaction [22], the overall energy required to transform the **DIHY-A** into **DIHY-B** is only 5.6 kcal/mol. The same isomerization process was excluded for the enamide hydrogenation because of the high activation energy required in order to form the **DIHY-A-B**‡ transition state (13.1 kcal/mol relative to **DIHY-A**). Similarly the C → D isomerization requires 6.6 kcal/mol in order to form **DIHY-D** starting from the **DIHY-C** intermediate. It is noteworthy that similar non-chelating species have been confirmed experimentally by low-temperature NMR for the related case of the enamide hydrogenation [28], but their involvement in the reaction pathway is unclear. In the present case, this pathway is favored due to the easier dissociation of the olefin from the strained chelate leading to a structure that is, in the case of the isomerization of A → B, 4.2 kcal/mol more stable and in the case of C → D isomerization 2.1 kcal/mol exothermic. After correction for zero-point and thermal energies, both processes are essentially barrierless.

4. Conclusions and outlook

The overall geometry of the transition structures and intermediates involved in the reaction pathway for the Rh(I) catalyzed hydrogenation of acrylamides closely resembles the ones determined previously for the case of the enamide hydrogenation [2–7,22]. The main differences in the structures and energetics of the reaction can be traced to the smaller ring size of the chelate, which leads to a weaker coordination of the olefin to the metal, and the differences in the model system under study here, notably the absence of a second acceptor. Together, these lead to higher relative free energies of the species involved in the pathway. This has important consequences for the overall reaction because an isomerization between the pathways now becomes energetically competitive. This possibility has not been described for the enamide reaction, presumably because it involves a dissociation of the olefin from the metal, which would render it energetically inaccesible in that case. As a result, the overall mechanism of the acrylamide reaction is found to proceed through formation of the octahedral metal dihydride complex through an approach of molecular hydrogen parallel to the P–Rh–C bond (A and C pathways), followed by an isomerization to the dihydride complexes where the hydrogens are aligned along the P–Rh–O axis. Irreversible hydride transfer then completes the reaction. Although in the model system under study, hydride transfer to the β-carbon is preferred by 3 kcal/mol, it is known that this preference is easily reversed based on the electronic character of additional ligands [7].

Based on the results presented here and in contrast to the case of the enamide substrate, the transition structure for the hydride transfer does not appear to be the rate determining step. Although this finding will have to be confirmed in studies of more realistic ligand and substrate systems, it does have important consequences for the design of chiral ligands for enantioselective hydrogenations. In analogy to computational and detailed experimental studies of the hydrogenation of the enamide substrate [2,22], no conclusive statement on whether the transition structures for the isomerization or the formation of the dihydride complex are relevant for the rate- and stereoselecting step is possible. This question will be addressed by the Q2MM parameterization of a transition state force field for all three relevant transition structures (**MOLH2**‡, **DIHY**‡, and isomerization) and comparison with experimental results. These studies are currently ongoing and will be published in due course.

Acknowledgements

We gratefully acknowledge financial support of this work by the Petroleum Research Fund (Grant PRF#47810-AC1), the National Science Foundation (NSF CHE0833220) and the Notre Dame Zahm Research Travel Fund, as well as generous allocation of computational resources by the TeraGrid (Grant TG-CHE090124) and the Center for Research Computing at the University of Notre Dame. Research was funded in part through the Northwest Indiana Computational Grid award from the Department of Energy grant #DE-FG52-06NA2689.

Appendix A. Supplementary data

Supplementary data associated with this article can be found, in the online version, at doi:10.1016/j.molcata.2010.02.026.

References

[1] W. Zhang, Y. Chi, X. Zhang, Acc. Chem. Res. 40 (2007) 1278–1290.
[2] C.R. Landis, J. Halpern, J. Organomet. Chem. 250 (1983) 485–490.
[3] S. Feldgus, C.R. Landis, J. Am. Chem. Soc. 122 (2000) 12714–12727.

[4] S. Feldgus, C.R. Landis, Catal. Met. Complex. 25 (2002) 107–135.
[5] P.J. Donoghue, P. Helquist, P.O. Norrby, O. Wiest, J. Chem. Theor. Comp. 4 (2008) 1313–1323.
[6] P.J. Donoghue, P. Helquist, P.O. Norrby, O. Wiest, J. Am. Chem. Soc. 131 (2009) 410–411.
[7] P.J. Donoghue, P. Helquist, O. Wiest, J. Org. Chem. 72 (2007) 839–847.
[8] I.D. Gridnev, T. Imamoto, Comm. Chem. (2009) 7447–7464, and references cited therein.
[9] E. Keinan, D. Perez, J. Org. Chem. 52 (1987) 2576–2580.
[10] K.Y. Koltunov, S. Walspurger, J. Sommer, Eur. J. Org. Chem. (2004) 4039–4047.
[11] H.M. Ali, A.A. Naiini, J. Brubaker, C. H, Tetrahedron Lett. 32 (1991) 5489–5492.
[12] T. Hayashi, N. Kawamura, Y. Ito, J. Am. Chem. Soc. 109 (1987) 7876–7878.
[13] T. Sturm, W. Weissensteiner, F. Spindler, Adv. Synth. Catal. 345 (2003) 160–164.
[14] Y. Wang, T. Sturm, M. Steurer, V.B. Arion, K. Mereiter, F. Spindler, W. Weissensteiner, Organometallics 27 (2008) 1119–1127.
[15] K.B. Hansen, Y. Hsiao, F. Xu, N. Rivera, A. Clausen, M. Kubryk, S. Krska, T. Rosner, B. Simmons, J. Balsells, N. Ikemoto, Y. Sun, F. Spindler, C. Malan, E.J.J. Grabowski, J.D. Armstrong III, J. Am. Chem. Soc. 131 (2009) 8798–8804.
[16] Z. Yang, M. Ebihara, T. Kawamura, J. Mol. Catal. A 158 (2000) 509–514.
[17] M. Ahlquist, M. Gustafsson, M. Karlsson, O. Axelsson, O.F. Wendt, Inorg. Chim. Acta 360 (2007) 1621–1627.
[18] A.D. Becke, J. Chem. Phys. 98 (1993) 5648–5652.
[19] P.J. Hay, W.R. Wadt, J. Chem. Phys. 82 (1985) 270–283.
[20] P.J. Hay, W.R. Wadt, J. Chem. Phys. 82 (1985) 299–310.
[21] W.R. Wadt, P.J. Hay, J. Chem. Phys. 82 (1985) 284–298.
[22] C.R. Landis, P. Hilfenhaus, S. Feldgus, J. Am. Chem. Soc. 121 (1999) 8741–8754.
[23] M.J. Frisch, H.B. Schlegel, G.E. Scuseria, M.A. Robb, J.R. Cheeseman, J.A. Montgomery, Jr., T. Vreven, K.N. Kudin, J.C. Burant, J.M. Millam, S.S. Iyengar, J. Tomasi, V. Barone, B. Mennucci, M. Cossi, G. Scalmani, N. Rega, G.A. Petersson, H. Nakatsuji, M. Hada, M. Ehara, K. Toyota, R. Fukuda, J. Hasegawa, M. Ishida, T. Nakajima, Y. Honda, O. Kitao, H. Nakai, M. Klene, X. Li, J.E. Knox, H.P. Hratchian, J.B. Cross, V. Bakken, C. Adamo, J. Jaramillo, R. Gomperts, R.E. Stratmann, O. Yazyev, A.J. Austin, R. Cammi, C. Pomelli, J.W. Ochterski, P.Y. Ayala, K. Morokuma, G.A. Voth, P. Salvador, J.J. Dannenberg, V.G. Zakrzewski, S. Dapprich, A.D. Daniels, M.C. Strain, O. Farkas, D.K. Malick, A.D. Rabuck, K. Raghavachari, J.B. Foresman, J.V. Ortiz, Q. Cui, A.G. Baboul, S. Clifford, J. Cioslowski, B.B. Stefanov, G. Liu, A. Liashenko, P. Piskorz, I. Komaromi, R.L. Martin, D.J. Fox, T. Keith, M.A. Al-Laham, C.Y. Peng, A. Nanayakkara, M. Challacombe, P.M.W. Gill, B. Johnson, W. Chen, M.W. Wong, C. Gonzalez, J.A. Pople, G.W.T. Gaussian 03; Revision E.01, Gaussian, Inc., Wallingford, CT, 2004.
[24] A.S.C. Chan, J.J. Pluth, J. Halpern, Inorg. Chim. Acta 37 (1979) L477–L479.
[25] A.S.C. Chan, J.J. Pluth, J. Halpern, J. Am. Chem. Soc. 102 (1980) 5952–5954.
[26] B. Mcculloch, J. Halpern, M.R. Thompson, C.R. Landis, Organometallics 9 (1990) 1392–1395.
[27] A.L. Sargent, M.B. Hall, M.F. Guest, J. Am. Chem. Soc. 114 (1992) 517–522.
[28] T. Imamoto, K. Yashio, K.V.L. Crepy, K. Katagiri, H. Takahashi, M. Kouchi, I.D. Gridnev, Organometallics 25 (2006) 908–914.